Evolution of superclusters and delocalized states in GaAs_{1−x}N_{x}

B. Fluegel, K. Alberi, D. A. Beaton, S. A. Crooker, A. J. Ptak, and A. Mascarenhas

Phys. Rev. B **86**, 205203 — Published 21 November 2012

DOI: 10.1103/PhysRevB.86.205203

Evolution of superclusters and delocalized states in $GaAs_{1-x}N_x$

B. Fluegel[1], K. Alberi[1], D. A. Beaton[1], S.A. Crooker[2], A. J. Ptak[1], and A. Mascarenhas[1]

[1] National Renewable Energy Laboratory, 15013 Denver West Blvd., Golden, CO 80401
[2] National High Magnetic Field Laboratory, Los Alamos National Laboratory, Los Alamos, NM 87545

The evolution of individual nitrogen cluster bound states into an extended state infinite supercluster in dilute $GaAs_{1-x}N_x$ was probed through temperature and intensity-dependent, time resolved and magneto-photoluminescence (PL) measurements. Samples with compositions less than 0.23% N exhibit PL behavior that is consistent with emission from the extended states of the conduction band. Near a composition of 0.23% N, a discontinuity develops between the extended state PL peak energy and the photoluminescence excitation absorption edge. The existence of dual localized/delocalized state behavior near this composition signals the formation of a N supercluster just below the conduction band edge. The infinite supercluster is fully developed by 0.32% N.

Introduction

Substitutional alloying provides an effective means of modifying the bandstructure of binary semiconductor compounds and typically results in a continuous change of the associated optical and electrical properties between the values of the endpoint constituents. It is known, however, that some isoelectronic substituents can produce discontinuous changes in electronic properties in the dilute alloy limit. $GaAs_{1-x}N_x$ exhibits a prime example of this phenomenon. Isolated nitrogen (N) atoms form a resonant state 150-180 meV above the conduction band edge of GaAs, and a continuous reduction in the bandgap energy is observed as a function of N doping concentration.[1,2,3,4] Additional modifications to the bandstructure are observed at N concentrations as low as 0.009%.[5] Simultaneously, the statistical formation of N pairs and clusters also produces trap states just below the conduction band edge. In photoluminescence (PL) studies, a series of sharp excitonic emission lines from these localized states remains fixed in energy for N compositions $\leq$ 0.1% N. This behavior is remarkably different at slightly higher N concentrations (> 0.4%), where excitonic emission from the N cluster states occurs as a single broad band that tracks the falling bandgap much like a conventional semiconductor alloy[6,7]. Recent experiments have shown that there is a sudden and discontinuous shift between these two N concentration regimes.[7] At both low (<0.1%) and high (> 0.4%) N concentrations, PL emission from extended states coincides with the band edge critical point energy, as measured by electromodulated reflectance (ER).[7] However, extended state emission was observed at energies well below the band edge in samples with intermediate compositions and was accompanied by an anomalous broadening of the ER linewidth.[7] This behavior was attributed to the percolation of individual localized N cluster

states into an infinite supercluster of extended states and the formation of a mobility edge. The exact nature of this transition is not well understood and requires further investigation.

This paper examines the localized to delocalized transition of N cluster states by investigating their PL emission characteristics. Temperature and intensity-dependent photoluminescence (PL), time-resolved PL (TRPL) and magneto-PL measurements are used to illustrate the evolution of an infinite supercluster and the emergence of a mobility edge at concentrations ≥ 0.2% N.

Experimental

Samples with N concentrations between 0.04% and 0.42% were grown by molecular beam epitaxy to thicknesses ~ 300 nm, and the compositions were determined by x-ray diffraction. Further details of the growth can be found in Ref. 8. The samples were very homogeneous with a constant PL spectral shape over regions of several mm. The temperature and intensity-dependent PL was excited with a continuous wave (cw) solid-state laser (515 nm) and detected with a 0.5 m spectrometer and a cooled Si charge-coupled device (CCD) array, with the sample mounted on the cold finger of an optical cryostat. Photoluminescence excitation (PLE) measurements were performed at 2 K with the sample in He vapor using a scanning, continuous wave, power-stabilized Ti:sapphire laser. At concentrations ≤ 0.12% N, it was possible to verify the PLE by measuring the absorption of the exciton peak using broad PL emitted from the substrates. Time-resolved PL measurements were carried out with a mode-locked Ti:sapphire laser at 2 MHz repetition rate that was tuned near resonance to the bandgap, and the PL signal was detected by a photon counting streak camera. Magneto-PL measurements were performed in the 60-T long-pulse magnet at the National High Magnetic

Field Laboratory (Los Alamos). PL was excited by a solid-state laser (515 nm) and collected through an optical fiber coupled to the sample cooled with liquid N_2.

Results

The discontinuity between the PLE absorption edge and the extended state PL emission in dilute $GaAs_{1-x}N_x$ is highlighted through comparison of low temperature pulsed-excitation PL and cw-excitation PLE spectra in Fig. 1. The PLE spectra shown in Fig. 1(a-c) for samples with N concentrations between 0.12% and 0.32% depict the spectrally sharp absorption edge associated with the high joint density of states (DOS) above the band edge. Detection was made either at a high-energy cluster peak lying just below the band edge or at a fully broadened band in the case of higher N concentrations. The PLE results were nearly independent of the choice of the detection spectral range. Although it is possible to detect PL from peaks labeled *A* and *B* in the PL spectra of Fig. 1 at higher temperatures and excitation densities, as discussed below, this did not result in sharper PLE features. The PLE curves were analyzed using a lineshape of excitonic absorption modified by phenomenological broadening terms for the exciton and continuum[9]. The band gap energies extracted from samples grown over a wide range of compositions, displayed in Fig. 1(d), follow a smooth trend that is consistent with previously published absorption, PLE and ER data.[6,7,10] By contrast, the time integrated PL emission spectra measured under pulsed excitation shown in Fig. 1 do not follow this same trend. At 2 K there is a strong competition for emission between the localized and delocalized states. Assessment of the PL characteristics at low and high excitation intensities therefore allows for precise identification of the delocalized states. For low pulsed excitation intensities (ultrafast Ti:sapphire laser, 1 $\mu J/cm^2$), carriers quickly

thermalize to N cluster bound states, and emission originates mainly from excitons localized at these states. Photogeneration of non-equilibrium carriers under high pulsed excitation intensities (20 $\mu J/cm^2$) is necessary to populate the higher-lying extended states. While the energy of the extended state PL emission closely tracks the PLE curves at 0.12% and 0.32% N, it deviates below the PLE curve for the 0.23% sample. This deviation exactly follows the 80 K PL/ER trend that was previously reported.[7] It can be seen in Fig. 1(d) where the cw-excited PL energies from Ref. 7 are reproduced for comparison with the PLE energies. The PL peak associated with emission from extended states of N concentrations below this PL/PLE deviation will be labeled *A* and those from concentrations above it will be labeled *B*.

Temperature and intensity-dependent PL trends provide additional insight into the distribution of localized and extended states around this discontinuity. Figure 2 shows PL spectra measured under cw excitation at low (3 mW) and high (75 mW) powers over a range of temperatures. The qualitative trends follow those obtained from the low temperature time integrated PL measurements presented in Fig. 1. At low temperatures and low-intensity excitation conditions, PL is mainly emitted from low energy localized N cluster states. Higher intensity excitation and/or higher temperatures are needed to populate the extended states that correspond to peaks *A* and *B*. The temperature and power dependence can be understood by considering the relative concentration and the exciton localization energy of the different cluster ($n \geq 2$) states in a dilute alloy of concentration $x << 1$. For a random placement of impurities on the lattice, the density of clusters of size n will have a dependence on x whose leading term goes as x^n. Larger clusters will therefore be more dilute than smaller ones, but their concentration will be more sensitive to x. Because larger clusters bind excitons

more strongly, recombination of those excitons corresponds to the lower energy peaks in the PL spectra of Fig. 2. Two additional salient observations can thus be made from these spectra. Firstly, at low temperatures emission from the localized N cluster states at the highest energies predominates, whereas at higher temperatures emission from the localized cluster states at lower energies predominates. This is evident from comparison of the 3 mW spectra measured at 5 K and 70 K and can be understood within the context of the trap filling process. Photogenerated carriers initially fall from the conduction band into spatially nearest bound states. Because the N cluster states at higher energy are more prevalent than those at lower energies, a greater number of states at higher energies are preferentially occupied by photogenerated carriers. There is not enough thermal energy at low temperatures for carriers trapped at these bound states to diffuse to farther lying lower energy states, and the emission therefore reflects the energetic distribution of excitons at N cluster states. Higher temperatures, on the other hand, provide enough thermal energy for subsequent diffusion processes, and carriers are able to reach and radiatively recombine from the farther lying deeper states.

Secondly, at low temperatures peak *A* for samples with 0.04% and 0.12% N concentrations can be excited under high intensity cw excitation, whereas peak *B* for samples with 0.23% and 0.32% N concentrations cannot. This suggests that there is a difference in the redistribution mechanism of photogenerated carriers between the two N concentration regimes. In the samples with low N concentrations ($\leq$ 0.12%), and under high-intensity excitation, preferential filling and saturation of N cluster bound states results in the buildup of carrier population in the conduction band. The saturating effect is partly due to the low concentration

of N clusters, but also to the incomplete diffusion of conduction band electrons to spatially separated clusters as discussed above. Thus, the faster radiative recombination rate from extended states at the conduction band leads to the predominance of peak *A*. The energies of the extended state PL peaks *A* and *B* extracted from the time integrated PL measurements at 2 K are marked with arrows in Fig. 2 for comparison. In the case of samples with high N concentrations (≥ 0.23%), the N cluster bound states are also populated, yet higher density excitation does not result in their saturation and the buildup of carriers in the extended states. These extended states are initially populated from carriers photogenerated in the conduction band, just as the high energy localized N cluster states are populated in the samples with low N concentrations. However, the extended nature of these supercluster states allows for subsequent redistribution of carriers into lower energy localized states, where carriers consequently remain trapped until they radiatively recombine. This set of N supercluster extended states below the conduction band therefore aids in the redistribution of photogenerated carriers to the lowest energy localized states. Furthermore, the density of the latter can be much higher in the 0.23% sample compared to the 0.12% sample as discussed above. The two effects make it more difficult to saturate the localized N states, and so peak *B* cannot be observed at low temperatures unless extreme non-equilibrium carrier concentrations are generated such as in the case of pulsed excitation. Thermally populating the supercluster states is also possible, and so peak *B* is visible at temperatures above ~40 K. The more efficient relaxation and diffusion in samples with $x \geq 0.23\%$ supports the conclusion that the states that contribute to peak *B* emission are spatially extended.

Magneto-PL measurements at elevated temperatures offer confirmation of the extended nature of peaks *A* and *B*. In order to ensure that for all samples the delocalized state is highly populated by the fiber-coupled laser excitation, a cw power density similar to the solid curves in Fig. 2 and a temperature of 115 K were used. Figures 3(a-d) display the PL spectra measured under a magnetic field ranging from 0 T to 30 T. Along with the major peaks from the $GaAs_{1-x}N_x$ epilayers, weak signals from the GaAs substrate are also observed in some of the spectra. Both peaks *A* and *B* blue shift with increasing magnetic field, as is expected for extended state behavior.[11] The magneto-PL dispersion curves are shown in Fig. 3(e). Localized N cluster states, by contrast, are well known to show no magneto-dispersion.[12] Peak *B* has a slightly weaker dispersion than peak *A*. This may be related to the percolation threshold, but is likely also part of a broader trend observed in higher concentrations[13,14].

TRPL measurements also help distinguish between localized and delocalized states.[7,15] Figure 4 shows time decay curves measured from deep N cluster states in a range of samples where peak *A* transitions to peak *B*. The spectral range is denoted by the arrows labeled "2" in the 1 $\mu J/cm^2$ spectra presented in Figs. 1(a-c). In all samples, slow ns decay times associated with carrier trapping at localized states are observed. The PL decay curves measured for peaks *A* and *B*, denoted by the arrow labeled "1" in Figs. 1(a-c), are shown in Fig. 5. Under low excitation densities (1 $\mu J/cm^2$, Fig. 5(a)), the samples with 0.12% and 0.32% N concentrations both exhibit fast decay times that are characteristic of extended states. These decay times are plotted in the inset of Fig. 5(a). The decay time of the 0.23% sample at the same low excitation intensity, however, is much slower and directly supports the existence of localized behavior in the energy range of peak *B*. On the other hand in Fig. 5(b), for all the samples,

decay curves measured in the spectral region 1 under high excitation densities (20 μJ/cm^2) all exhibit fast decay rates. The decay times are shown in the inset of Fig. 5(b). The transformation from slow to fast decay times in the 0.23% N sample as the excitation intensity is increased indicates that there is dual localized/delocalized behavior among the associated states in this sample but that the majority are extended in nature. Finally, the fast time decay for peak *B* originating under high-intensity excitation is preceded by a slightly slower decay rate. This can be understood through a saturation of the more delocalized states.

A simple modeling of the decay rates provides insight into this behavior and the carrier dynamics within the localized and extended N cluster states. The PL decay curves of the samples with N concentrations ≥ 0.23% can be reproduced if we assume that three levels exist: the host conduction band with a high DOS, a percolated N supercluster state just below the conduction band edge, and a set of dilute localized N cluster states at lower energies. These are shown schematically in the inset of Fig. 6. The time dependencies of the carrier concentrations, n_1, n_2, and n_3, of the three levels are governed by Eqs. 1-3, respectively.

$$\frac{dn_1}{dt} = -\frac{n_1}{\tau_1} + A(t) \qquad (1)$$

$$\frac{dn_2}{dt} = \frac{n_1}{\tau_1} - \frac{n_2}{\tau_{2r}} - \frac{n_2\left(1-\frac{n_3}{n_s}\right)}{\tau_2} \qquad (2)$$

$$\frac{dn_3}{dt} = -\frac{n_3}{\tau_{3r}} + \frac{n_2\left(1-\frac{n_3}{n_s}\right)}{\tau_2} \qquad (3)$$

The radiative lifetimes of the percolated N supercluster (τ_{2r}) and the localized N cluster states (τ_{3r}) are both taken as 2 ns. The transfer times between the conduction band and supercluster

(τ_1) and between the supercluster and the localized N cluster states (τ_2) are both set at 100 ps. *A(t)* is an ultrafast generation rate, and the localized N cluster states saturate at the population of n_S. The calculated decay curve for the carrier population in the conduction band (not shown) follows a simple exponential decay given by the carrier transfer to the lower energy supercluster and localized N cluster states. The decays of these two levels, calculated for a generation rate whose integrated total is not large compared to n_S, are shown in the dashed curves of Fig. 6: both populations rise with time τ_1 and decay exponentially. For the supercluster state this decay is the rapid transfer time, whereas the N cluster states have a long decay commensurate with their ns radiative lifetimes. These dashed curves explain the fast and slow PL decays exemplified by the 0.32% N sample in Fig. 5(a) and Fig. 4. When the generation rate is higher, carrier transfer to localized N cluster states quickly bottlenecks as modeled by the saturation term in Eqs. 2-3. Electrons in the N supercluster are then forced to radiatively recombine at the ns timescale, leading to the slow initial decay calculated in the solid n_2 curve of Fig. 6 and observed in the TRPL curves of peak B shown in Fig. 5(b). In both figures, once the localized N cluster states start to become depopulated through radiative recombination, fast carrier transfer to these states from the supercluster resumes, and the population decay rate increases.

Discussion

Within the framework of percolation theory, the PL emission characteristics detailed above provide information about how localized N cluster states evolve into an infinite supercluster.[16,17] The number and configuration of the atoms that comprise the N clusters determines their energy, with the larger ones having a greater binding energy. At ultra-dilute concentrations, most clusters that form will statistically contain very few N atoms. The

exciton binding energy to these clusters is relatively small, and so the relatively large hole orbit around the trapped electron enables overlap of their wavefunctions at lower N concentrations. However, with increasing N concentration the rapidly downward shifting conduction band readily overtakes and hybridizes with the smallest N cluster bound states before percolation can occur. Concurrently, the relative abundance of larger N cluster states with larger binding energies increases, and thus there comes a point where a percolation network of large clusters evolves into the formation of a supercluster before the conduction band overtakes it. The co-existence of both localized and delocalized emission behavior in the 0.23% sample suggests that this concentration is just past the percolation threshold. A percolated supercluster has started to form, which give rise to extended state behavior, but there are still isolated pockets of localized states at the same energy. The latter are filled first and account for the long decay times observed in the sample with 0.23% N under low-density excitation. As the N concentration is further increased, the supercluster becomes infinite, and only extended state behavior is observed.

From the percolation threshold onwards, supercluster states define the mobility edge as the boundary between localized and delocalized states. This is readily evident in the PL spectra shown in Fig. 2. Peak *A* is always separated from the majority of the lower energy localized states, indicating that it is a separate entity. Peak *B*, however, is always conjoined to the broad spectrum of localized state emission, with a mobility edge separating the two. This comparison is most evident in the 3 mW spectra measured at 60 K in Fig. 2.

In summary, a combination of temperature and intensity-dependent PL, TRPL and magneto-PL measurements was used to distinguish between emission from localized and delocalized states in dilute $GaAs_{1-x}N_x$ alloys. Very different behavior in the PL emission from delocalized states was observed in samples with compositions below and above 0.23% N. The results provide a detailed account of N supercluster formation in $GaAs_{1-x}N_x$ alloys near this composition.

Acknowledgements

We acknowledge the financial support of the Department of Energy Office of Science, Basic Energy Sciences under DE-AC36-08GO28308.

[1] D. J. Wolford, J. A. Bradley, K. Fry and J. Thompson, in *Proceedings of the 17th International Conference on the Physics of Semiconductors* (Springer-Verlag, New York, 1985), p. 627.

[2] M. Weyers, M. Sato, and H. Ando, Jpn. J. Appl. Phys., Part 2 **31**, L853 (1992).

[3] P. J. Klar, H. Grüning, W. Heimbrodt, J. Koch, F. Höhnsdorf, W. Stolz, P. M. A. Vicente, and J. Camassel, Appl. Phys. Lett. **76**, 3439 (2000).

[4] S. Francoeur, M. J. Seong, M. C. Hanna, J. F. Geisz, A. Mascarenhas, H. P. Xin, and C. W. Tu, Phys. Rev. B **68**, 075207 (2003).

[5] J. D. Perkins, A. Mascarenhas, Y. Zhang, J. F. Geisz, D. J. Friedman, J. M. Olson, and S. R. Kurtz, Phys. Rev. Lett. **82**, 3312 (1999).

[6] G. Bentoumi, V. Timoshevskii, N. Madini, M. Coté, R. Leonelli, J.-N. Beaudry, P. Desjardins, and R. A. Masut, Phys. Rev. B **70**, 035315 (2004).

[7] K. Alberi, B. Fluegel, D.A. Beaton, A.J. Ptak and A. Mascarenhas, *Phys. Rev. B*, **86**, 041201(R) (2012).

[8] Ptak, A.J. *et al*. A comparison of MBE- and MOCVD-grown GaInNAs. *J. Cryst.Growth* **251**, 392–398 (2003).

[9] R. J. Elliott, Phys. Rev. **108**, 1384 (1957).

[10] H. Grüning, L. Chen, Th. Hartmann, P. J. Klar, W. Heimbrodt, F. Höhnsdorf, J. Koch, and W. Stolz, phys. stat. sol. (b) **215**, 39 (1999).

[11] See, for example, N. Miura, *Physics of Semiconductors in High Magnetic Fields* (Oxford University Press, Oxford, 2008).

[12] Y.J. Wang, X. Wei, Y. Zhang, A. Mascarenhas, H.P. Xin, Y.G. Hong and C.W. Tu, Appl. Phys. Lett., **82**, 4453 (2003).

[13] F. Masia, A. Polimeni, G. Baldassarri Höger von Högersthal, M. Bissiri, M. Capizzi, P. J. Klar and W. Stolz, Appl. Phys. Lett. **82**, 4474 (2003).

[14] N. Mori, K. Hiejima, H. Kubo, A. Patane and L. Eaves, AIP Conf. Proc. **1399**, 23 (2011).

[15] X. D. Luo, J. S. Huang, Z. Y. Xu, C. L. Yang, J. Liu, W. K. Ge, Y. Zhang, A. Mascarenhas, H. P. Xin, and C. W. Tu, Appl. Phys. Lett. **82**, 1697 (2003).

[16] A.L. Efros, Sov. Phys. Usp. **21**, 746 (1978).

[17] A. Klochikhin, A. Reznitsky, S. Permogorov, T. Breitkopf, M. Grün, M. Hetterich, C. Klingshirn, V. Lyssenko, W. Langbein, and J. M. Hvam, Phys. Rev. B **59**, 12947 (1999).

FIG. 1 (Color online). PL spectra taken under low and high pulsed excitation densities (solid lines) and the corresponding PLE spectrum (dashed lines) are shown for samples with a) 0.12% N, b) 0.23% N and c) 0.32% N. The horizontal arrows marked "PLE" indicate the spectral regions that were detected for PLE; "1" and "2" are the regions over which TRPL decay curves were measured. The extracted 2K PLE bandgap energies and 80 K PL *A* or *B* peak energies (Ref. 7) are shown in d).

FIG. 2 (Color online). PL spectra measured over the temperature range 10 – 80 K for samples with N concentrations of a) 0.04% N, b) 0.12% N, c) 0.23% N and d) 0.32% N. The spectra measured under excitation powers of 3 mW (solid lines) and 75 mW (dashed lines) are not displayed on the same scale. Arrows indicate the energies of peaks *A* and *B* measured under pulsed excitation (Fig. 1) at 2 K for each sample.

FIG. 3 (Color online). PL spectra measured under a range of applied magnetic fields (0 – 30T) for samples with N concentrations of a) 0.04% N, b) 0.12% N, c) 0.23% N, d) 0.32% N. The magneto-dispersion curves of the peaks labeled *A* and *B* are shown in e).

FIG. 4 (Color online). PL decay curves measured at localized N cluster states over the spectral region marked with a horizontal arrow labeled "2" in Fig. 1 for samples with N concentrations of 0.12%, 0.23% and 0.32%. Measurements were performed at 1 $\mu J/cm^2$.

FIG. 5 (Color online). PL decay curves for N concentrations of 0.12%, 0.23% and 0.32% measured under excitation powers of a) 1 $\mu J/cm^2$ and b) 20 $\mu J/cm^2$. All decay curves were

measured in the spectral regions indicated by the horizontal arrows labeled "1" in Fig. 1. The insets show the decay times extracted from the single-exponential fits that are plotted as black lines in the main figures.

FIG. 6 (Color online). Theoretical population decay curves for carriers in the percolated N supercluster and localized N cluster states calculated from Eqs. 1-3. The time-integrated laser excitation into level 1 is equal to $2.5n_s$ for the dashed curves and $50n_s$ for the solid curves. A schematic of the relative energy positions of the three sets of states is shown in the inset.

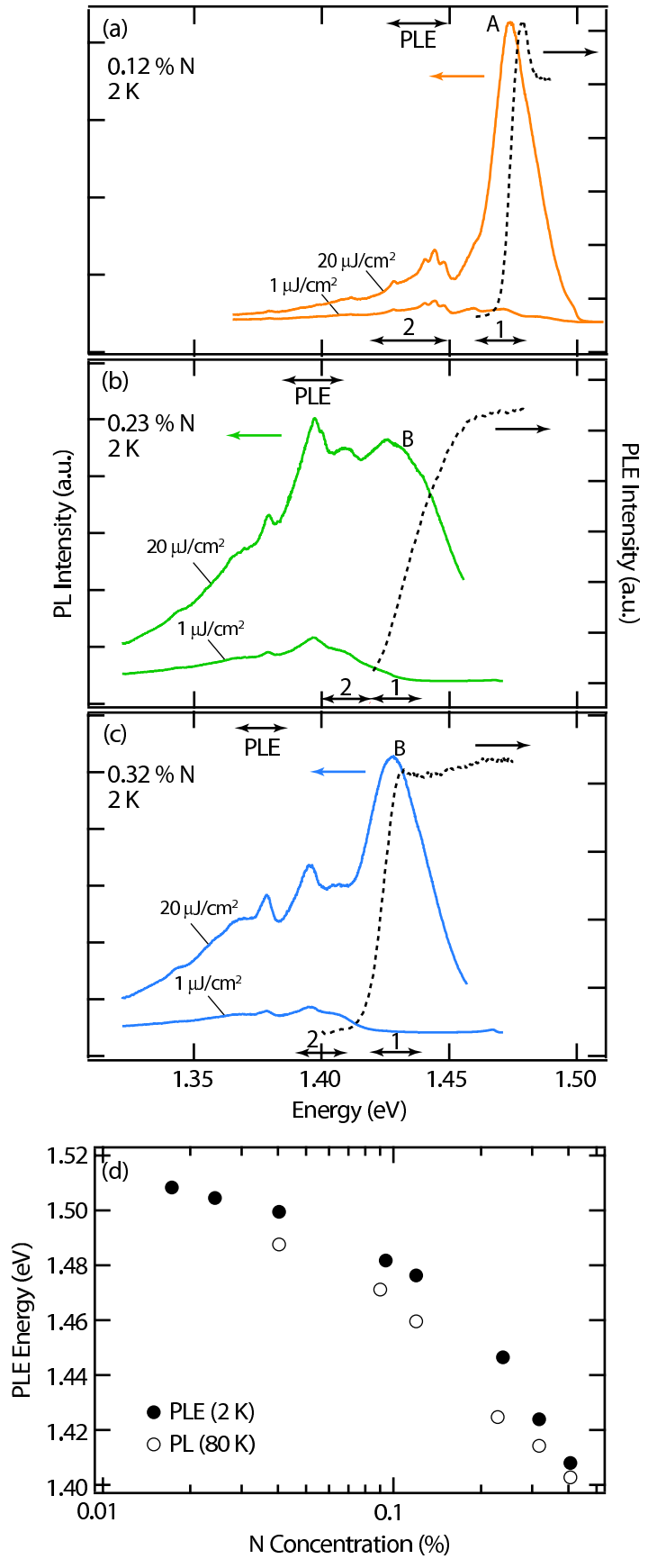

Figure 1 BV11956 24OCT2012

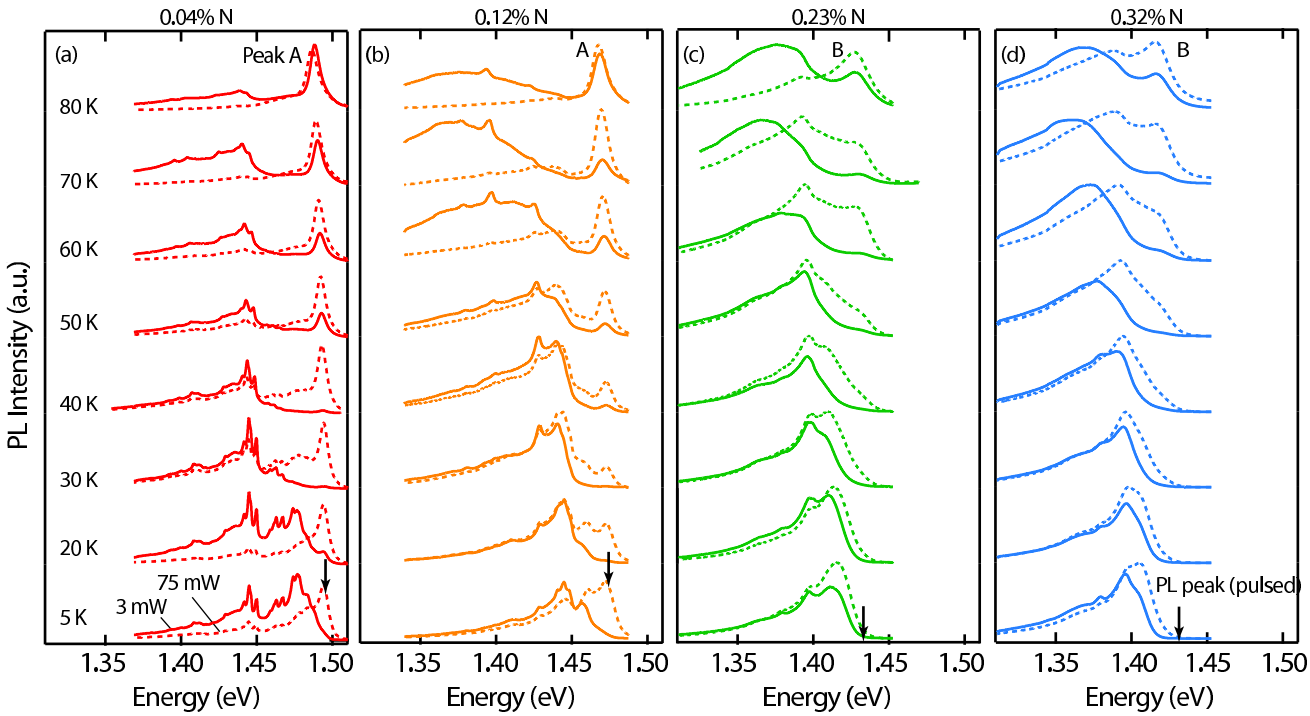

Figure 2 BV11956 24OCT2012

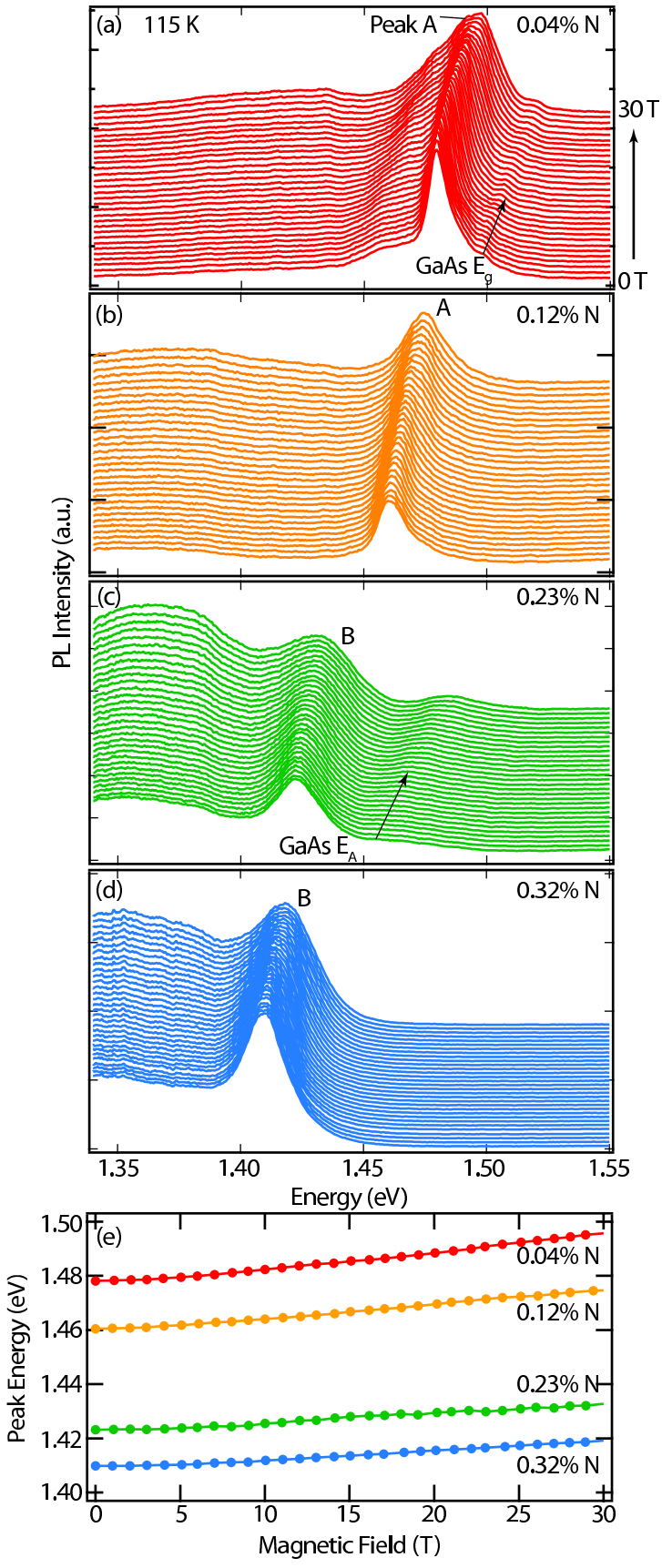

Figure 3 BV11956 24OCT2012

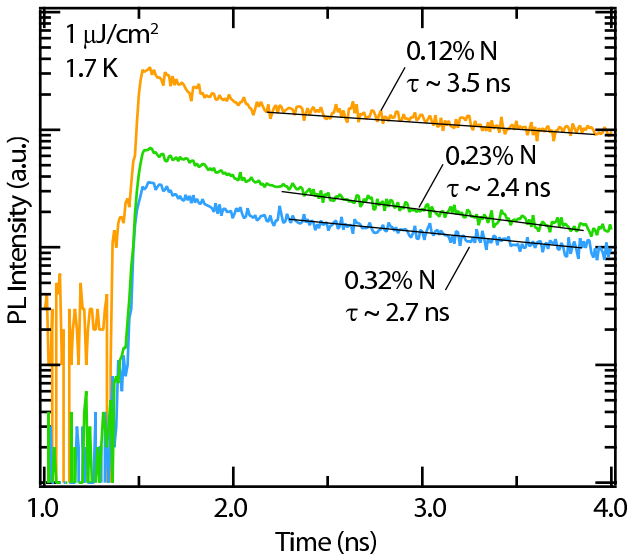

Figure 4 BV11956 24OCT2012

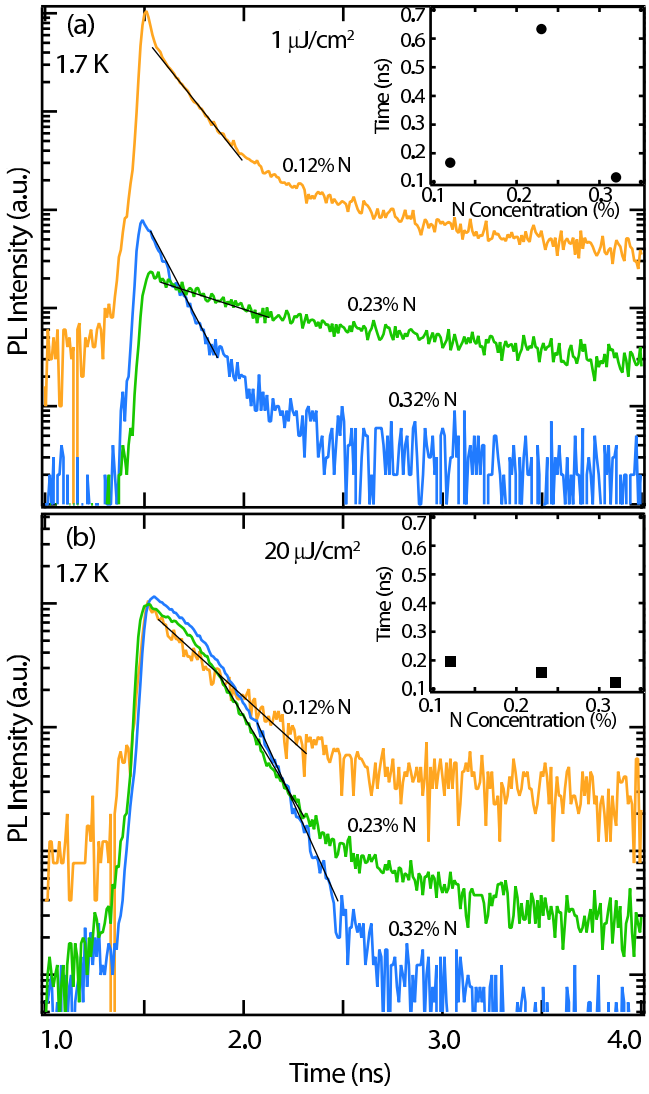

Figure 5 BV11956 24OCT2012

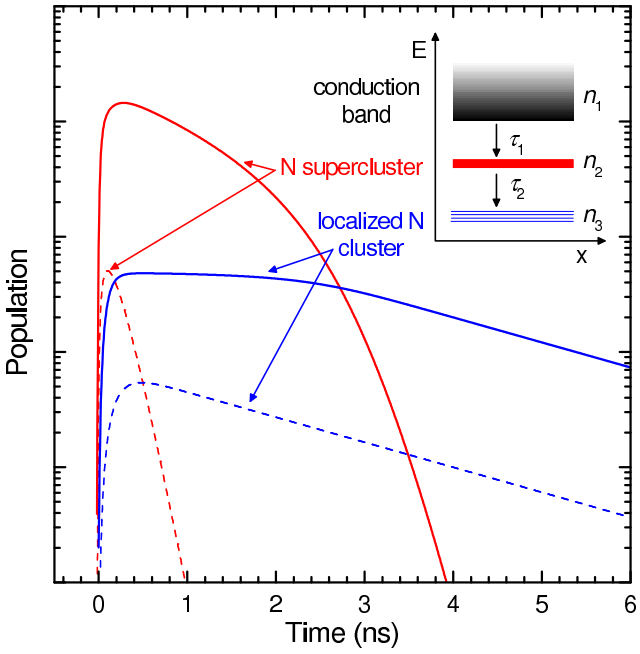

Figure 6 BV11956 24OCT2012